Biosensors and Bioelectronics 126 (2019) 207–213

Contents lists available at ScienceDirect

Biosensors and Bioelectronics

journal homepage: www.elsevier.com/locate/bios

An ultrasensitive electrochemical impedance-based biosensor using insect odorant receptors to detect odorants

Roshan Khadka[a,b], Nihan Aydemir[a,b], Colm Carraher[c], Cyril Hamiaux[c], Damon Colbert[c], Jamal Cheema[a,b], Jenny Malmström[b,d], Andrew Kralicek[c,*], Jadranka Travas-Sejdic[a,b,**]

[a] Polymer Electronic Research Centre, School of Chemical Sciences, The University of Auckland, 23 Symonds Street, Auckland 1023, New Zealand
[b] MacDiarmid Institute for Advanced Materials and Nanotechnology, Kelburn Parade, Wellington 6140, New Zealand
[c] The New Zealand Institute for Plant and Food Research Limited, Private Bag 92169, Auckland 1142, New Zealand
[d] Department of Chemical and Materials Engineering, University of Auckland, Auckland 1023, New Zealand

ARTICLE INFO

Keywords:
Insect odorant receptor
Liposome
Biosensor
Electrochemical impedance spectroscopy
Quartz crystal microbalance

ABSTRACT

Herein, we present that insect odorant receptors reconstituted into the lipid bilayers of liposomes can be successfully immobilized onto a gold surface and selectively and sensitively detect odorant molecules. The odorant receptors (OrXs) Or10a, Or22a, and Or71a from the common fruit fly, *Drosophila melanogaster*, were recombinantly expressed, purified and integrated into nano-liposomes (100–200 nm). These liposomes were covalently attached to the self-assembled monolayers (SAMs) of a 6-mercaptohexanoic acid (MHA)-modified gold surface. X-ray Photo Electron Spectroscopy (XPS) and Quartz Crystal Microbalance with Dissipation (QCM-D) measurements confirmed the successful modification of the gold surface and immobilization of liposomes. Atomic Force Microscopy (AFM) revealed that the liposomes were covalently attached to the surface without any disruption of vesicles. The liposomes tethered to the gold sensor surface were then treated with a range of known ligands of various concentrations. We demonstrated by Electrochemical Impedance Spectroscopy (EIS) that an OrX/liposome EIS sensor can sensitively and selectively detect its known ligand to femtomolar concentrations by detecting a change in electrical signal upon binding. Our study is the first step towards using purified insect odorant receptors alone in biosensors to enable the development of novel ultrasensitive volatile sensors for medical diagnostic, air quality, food safety and border security applications.

1. Introduction

Insects exhibit an unmatched sense of smell (Angioy et al., 2003) that is critical to how mates are attracted, food sources identified and hosts located (Ihara et al., 2013). Their unique odorant receptors (Kaupp, 2010) are the key to their extreme sensitivity and rapid detection of volatile chemical signals. These receptors are membrane proteins expressed within the olfactory sensory neurons present in the sensilla found on the surface of their antennae. In contrast to mammals that use G-protein coupled receptors (GPCRs) to smell (Kaupp, 2010), insects use a novel class of ligand-gated cation channel (Carraher, 2013) which are complexes (German et al., 2013) of an ion channel-forming subunit, Orco, and one of a family of highly divergent odorant "tuning" receptors, OrX. Studies on fly and mosquito OrX specificities suggest that insect OrXs respond to odorants in a combinatorial manner, with a specific odorant activating multiple OrXs, and each OrX being activated by multiple ligands (Carey et al., 2010; Hallem and Carlson, 2006; Wang et al., 2010).

These receptors are prime candidates as sensing elements for biosensors as they can distinguish diverse natural and synthetic volatile organic chemicals (VOCs) (Boyle et al., 2013; Marshall et al., 2010; Nowotny et al., 2014). However, their utility for biosensing is only just starting to be demonstrated. Insect OrXs have been expressed in cell lines to characterize their compound specificity and sensitivity (Montagné et al., 2015). These studies have used either intracellular fluorescent dyes or voltage clamp electrophysiology to detect changes in OrX/Orco ion channel activity in response to odorant binding to the OrX subunit. Cells expressing an OrX/Orco ion channel have been placed in devices and odorant binding detected by voltage clamp electrophysiological measurements (Misawa et al., 2010; Sato and

* Crossponding author.
** Crossponding author at: Polymer Electronic Research Centre, School of Chemical Sciences, The University of Auckland, 23 Symonds Street, Auckland 1023, New Zealand.
E-mail addresses: andrew.kralicek@plantandfood.co.nz (A. Kralicek), j.travas-sejdic@auckland.ac.nz (J. Travas-Sejdic).

https://doi.org/10.1016/j.bios.2018.10.043
Received 16 August 2018; Received in revised form 18 October 2018; Accepted 22 October 2018
Available online 23 October 2018
0956-5663/

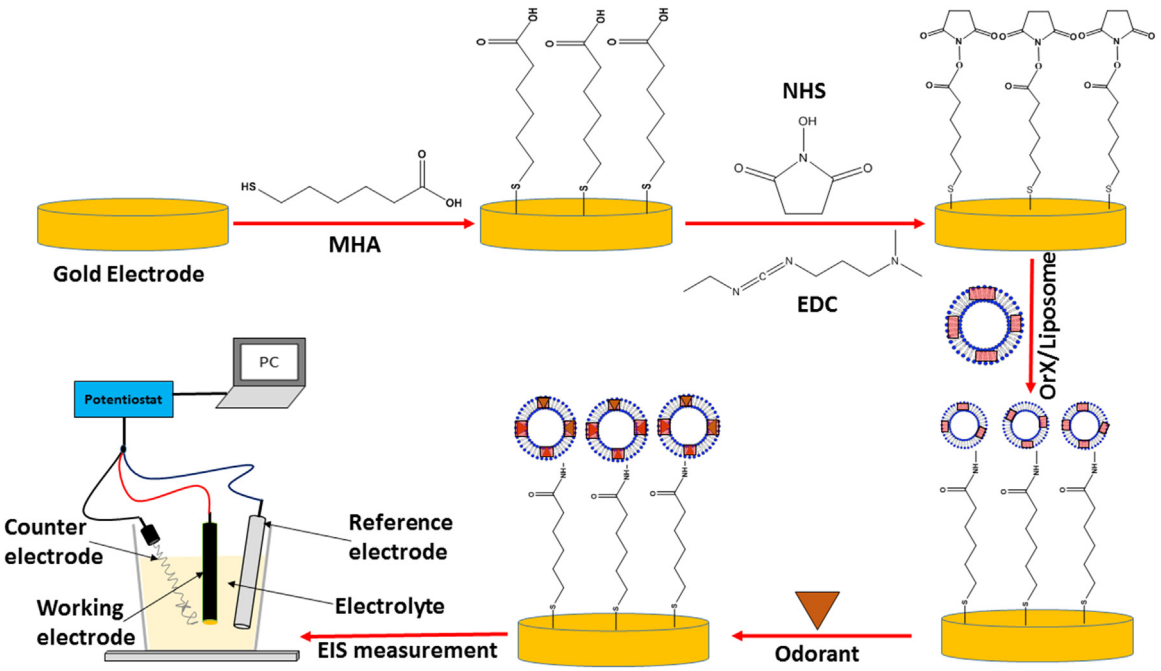

Scheme 1. Procedure to covalently link OrX/liposomes to gold electrodes, showing NHS-EDC coupled MHA incubation, OrX/liposomes immobilization, hybridization of target odorant ligand and EIS measurements in a three terminal electrochemical cell.

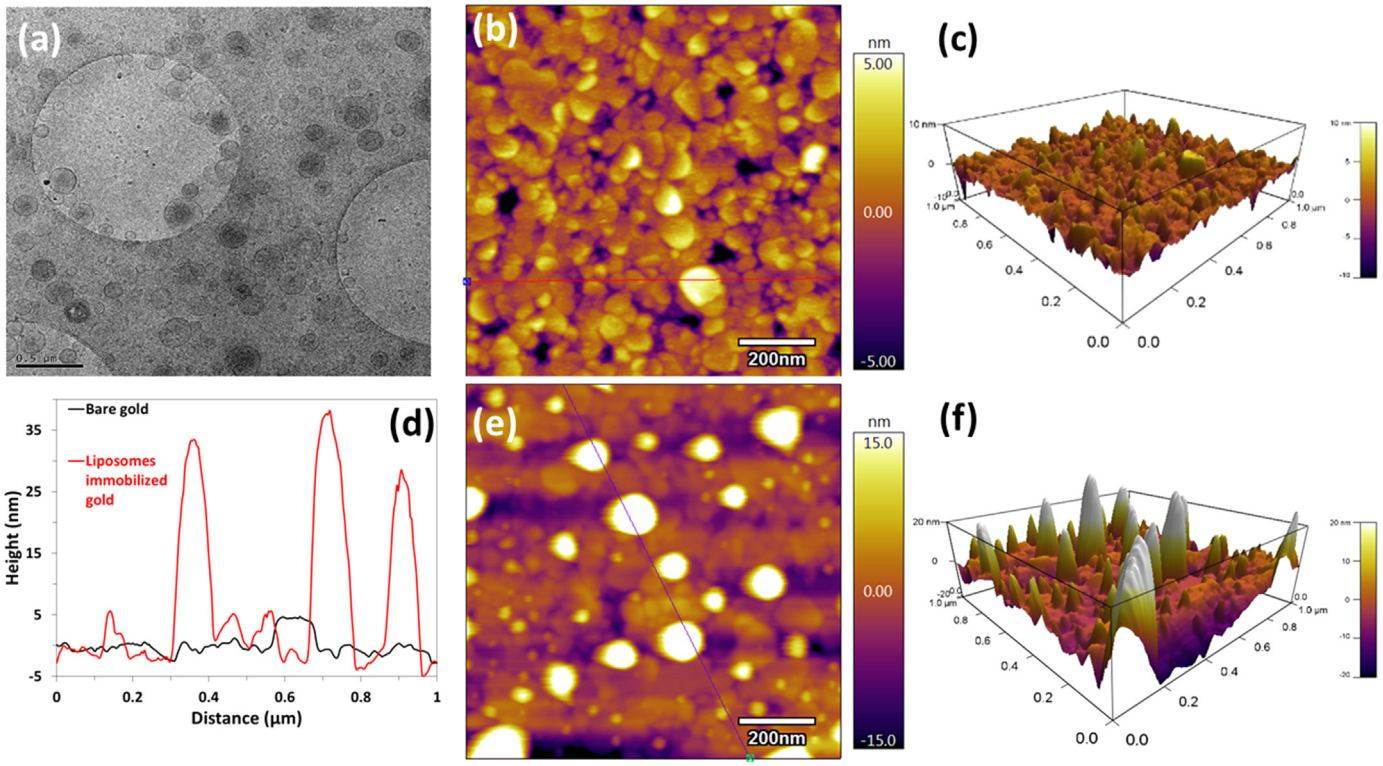

Fig. 1. Physical properties (size, shape and state) of Or10a/liposomes when attached to a solid substrate as investigated by TEM and AFM studies. (a) TEM image of the liposomes on a carbon grid, (b, c) AFM height and 3D image of bare gold surface (d) roughness profile of the bare and Or10a/liposome immobilized gold surface indicated by the marked line on AFM height images, (e-f) AFM height and 3D image of the Or10a/liposome immobilized gold surface, respectively.

Takeuchi, 2014), or by measuring calcium influx-induced fluorescence (Mitsuno et al., 2015). This latter approach has been further extended to create a cell-based sensor array (Termtanasombat et al., 2016). However, the drawback of these approaches is that they rely on the creation and maintenance of living cells that express an OrX/Orco ion channel.

In the case of mammalian odorant receptors (which are not ion channels), there are examples of purified receptors that have been coupled to different sensor platforms to detect odorant binding, such as electrochemical impedance spectroscopy (EIS) (Alfinito et al., 2013; Benilova et al., 2008b; Guo et al., 2015; Hou et al., 2007), surface plasmon resonance (SPR) (Benilova et al., 2008a; Cook et al., 2009;

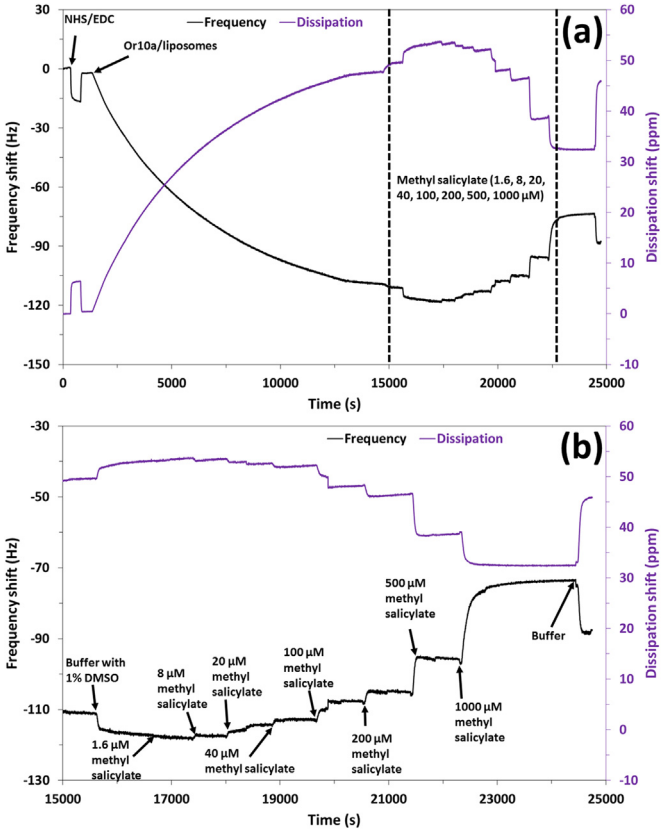

Fig. 2. Or10a/liposomes immobilized QCM-D biosensor showing the detection of methyl salicylate. (a) The change in frequency and dissipation of SAM-modified gold surface after NHS/EDC coupling, followed by Or10a/liposomes immobilization on the quartz crystal microbalance (QCM) and then binding of the target ligand methyl salicylate. (b) A close up view of the change in frequency and dissipation with increasing concentrations of methyl salicylate (1.6, 8, 20, 40, 100, 200, 500 and 1000 µM) for the Or10a/liposomes immobilized QCM sensor.

Kaiser et al., 2008), piezoelectric quartz crystal microbalance with dissipation (QCM-D) (Du et al., 2013; Sung et al., 2006), and carbon nanotube (CNT) and graphene field effect transistors (FETs) (Goldsmith et al., 2011; Park et al., 2012; Yang et al., 2017). To date there have been no papers published concerning the coupling of purified insect odorant receptors to any kind of sensor platform.

In 2013, we developed a protocol for the recombinant expression of insect OrX and Orco subunits using baculovirus-mediated expression in insect Sf9 cells, purified these subunits and reconstituted them into artificial liposomes (Carraher et al., 2013). Now we show that OrX/liposomes in the absence of Orco can be coupled to an EIS sensor platform to enable the selective and ultrasensitive (femtomolar or parts per quadrillion) detection of odorants.

Three odorant receptors from *Drosophila melanogaster*, namely Or10a, Or22a and Or71a, were integrated into the lipid bilayers of artificial liposomes and these OrX/liposomes were immobilized onto gold electrodes. Atomic Force Microscopy (AFM), Transmission Electron Microscopy (TEM), X-ray Photo Electron Spectroscopy (XPS), and QCM-D were applied to understand the various properties of the OrX/liposomes before and after binding the target compounds. QCM-D and EIS studies were then performed to characterize the sensitivity and selectivity of the OrX/liposomes for their target odorants. We show that an insect OrX EIS biosensor can detect target odorants ultrasensitively and selectively, and surprisingly does not require the presence of the Orco subunit to function.

2. Material and methods

2.1. Materials

6-Mercaptohexanoic acid (MHA), N-hydroxysuccinimide (NHS), 1-ethyl-3-((3-dimethylaminopropyl)-carbodiimide) (EDC), phosphate buffer saline (PBS) tablets, methyl salicylate, methyl hexanoate, ethyl hexanoate, E2-hexenal and 4-ethylguaiacol were obtained from Sigma-Aldrich. 1.6-mm diameter gold (Au) disk electrode, coiled platinum (Pt) wire electrode and leakless silver/silver chloride (Ag/AgCl) electrode were purchased from BASi for electrochemical measurements. Titanium/Gold (Ti/Au)-coated (~40 nm / 50 nm) microscope slides 25.4 × 76.2 × 1.1 mm were purchased from Deposition Research Lab, Inc. (DRLI) for AFM and XPS studies. 100 nm gold sensor crystals were purchased from ATA Scientific for conducting QCM-D measurements.

2.2. Methods

Detailed description for the preparation of purified OrX subunits and preparation of liposome associated OrX subunits are shown in Khadka et al. (2018) (Data in Brief, page 12–13).

2.2.1. Electrode preparation

Gold disk electrodes (1.6-mm diameter) were polished on a diamond pad with polishing alumina slurry for 1 min for each electrode. The polished electrodes were rinsed with deionized water (Milli-Q, 18.2 MΩ cm) followed by ultrasonication in ethanol (LR grade) and deionized water until the residual alumina slurry was completely removed from the electrodes. Chronoamperometry at − 1.4 V was applied to the electrodes to desorb the SAMs of the thiol present on the surface of the electrodes. This was performed for 30 s using a 0.1 M sodium hydroxide (NaOH) electrolyte solution in a 3-terminal electrochemical cell, Ag/AgCl (3 M NaCl, 0.209 V vs. SHE) reference electrode, coiled platinum wire as a counter electrode and gold disk as a working electrode, using a PalmSens3 potentiostat. Then, the electrodes were again rinsed with deionized water and ultrasonicated in ethanol and deionized water consecutively. Finally, cyclic voltammetry was performed for ten cycles between − 0.2 and 1.6 V, at a scan rate of 50 mV/s in 0.5 M sulphuric acid (H_2SO_4) solution to remove any other impurities (a 3-electrode cell, Ag/AgCl (in 3 M NaCl, 0.209 V vs. SHE) reference electrode, coiled platinum wire as a counter electrode and gold disk as a working electrode).

2.2.2. SAMs and EDC:NHS activation

2 mM MHA was prepared by dissolving 1.36 µL of MHA in 5 mL ethanol (AR grade). The cleaned electrodes were immersed into MHA solution and incubated overnight at room temperature. The next day, the electrodes were washed with ethanol and deionized water thoroughly in order to remove the unreacted acid. A 2:1 mol: mol ratio of EDC:NHS (100 mM EDC, 50 mM NHS) was prepared in 2 mL PBS (pH = 6.5) solution. Then, the electrode surfaces were covered with 100 µL of this solution at 28 °C for 1 h to activate the carboxylic (COOH) groups of the MHA.

2.2.3. Immobilization of OrX/liposomes on gold surfaces

All buffer solutions were filtered and degassed by flushing with N_2 for 30 min prior to use. PBS solution was prepared by immersing one tablet of PBS in 200 mL of milli-Q water and filtered using a 0.2-µm syringe filter. The pH of the prepared buffer solution was measured with a pH meter and adjusted to pH 7.4. Each liposome stock solution was diluted 100-fold for EIS, QCM-D, and XPS study and 10-fold for AFM and TEM study in PBS buffer solution (pH 7.4), and the -COOH-activated electrodes were incubated in that buffer solution at room temperature for 1 h. 100 µL of this dilution was incubated on a gold electrode which means there is a maximum of 0.1 µg or ~2 pmol of OrX molecules on the electrode. Then, the electrodes were washed

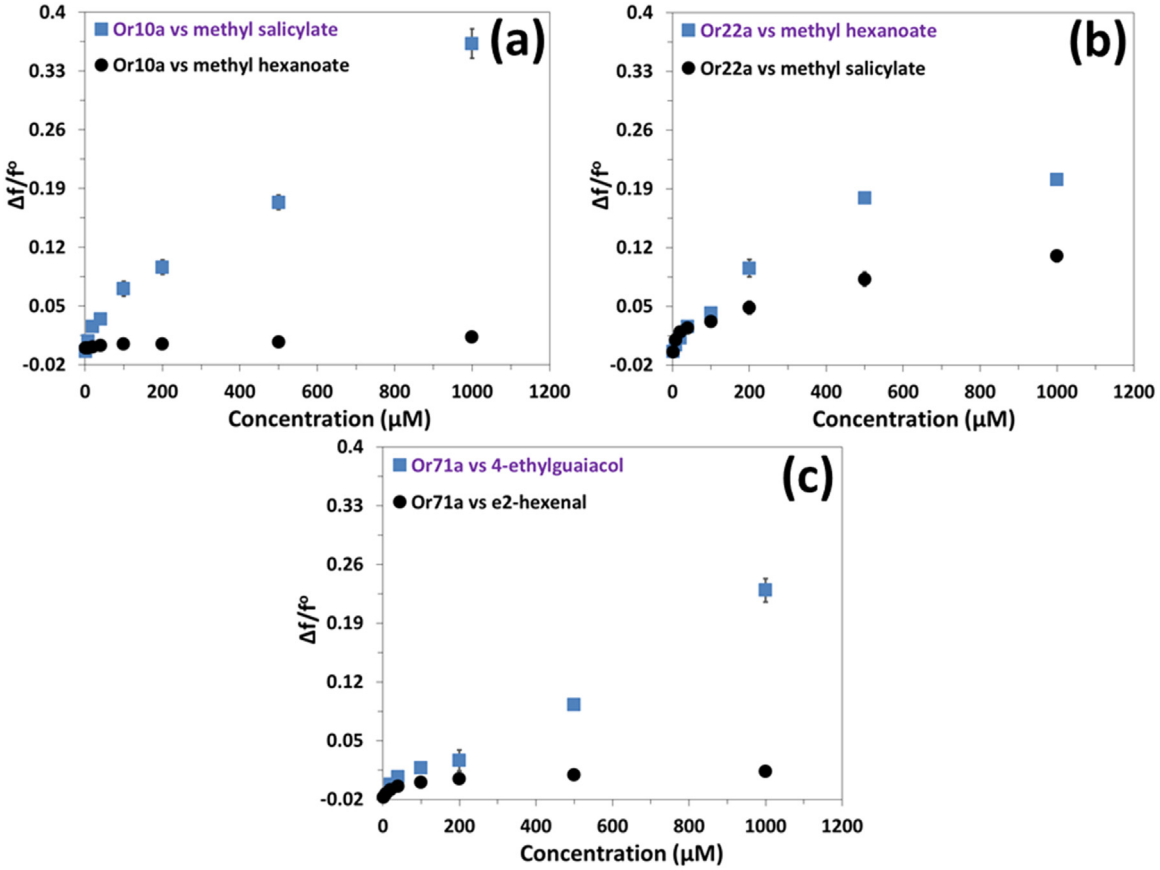

Fig. 3. Dose response curves showing specific detection of different ligands by each OrX/liposome immobilized QCM-D sensor. (a) Or10a/liposomes show selective detection of methyl salicylate (b) Or22a/liposomes show selective detection of methyl hexanoate with a reduced response to methyl salicylate (c) Or71a/liposomes show selective detection of 4-ethylguaiacol. Error bars; standard deviation (SD) were generated using two repeats.

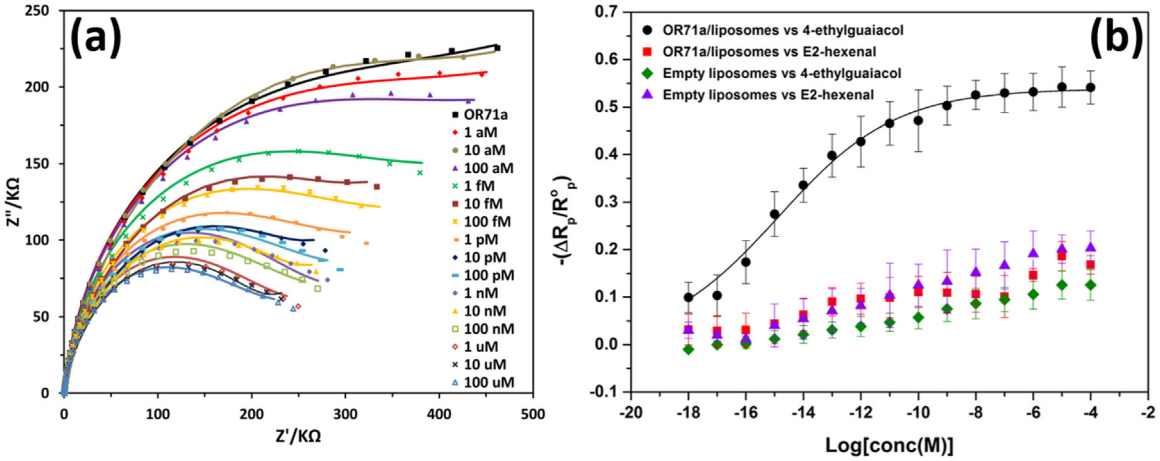

Fig. 4. Odorant detection using an Or71/liposome immobilized EIS sensor. (a) The Nyquist plot of an Or71a/liposomes coupled gold surface and binding of different concentrations of 4-ethylguaiacol (1 aM, 10 aM, 100 aM, 1 fM, 10 fM, 100 fM, 1 pM, 10 pM, 100 pM, 1nM, 10 nM, 100 nM, 1 μM, 10 μM and 100 μM) showing a decrease in impedance with increase in concentration of 4-ethylguaiacol; and (b) dose response curve for the Or71/liposome EIS sensor showing the change in normalized polarization resistance with increasing concentration of the positive ligand, 4-ethylguaiacol, as well as response to the negative ligand E2-hexenal. The response of an empty liposome EIS sensor to 4-ethylguaiacol and E2 hexenal is shown for comparison. Error bars; standard deviation (SD) were generated using four repeats.

extensively with PBS buffer solution to wash out any free liposomes.

2.2.4. Electrolyte and odorant preparation

PBS (pH 7.4) was used as an electrolyte to conduct electrochemical measurements. PBS was degassed for 15 min prior to electrochemical measurements. Odorant solutions of concentration ranging from 1 aM to 1 μM were prepared by sequential dilution in PBS containing 1% DMSO. OrX-immobilized electrodes were incubated in the relevant odorant solution for ~30 min each and washed gently with PBS before EIS measurements.

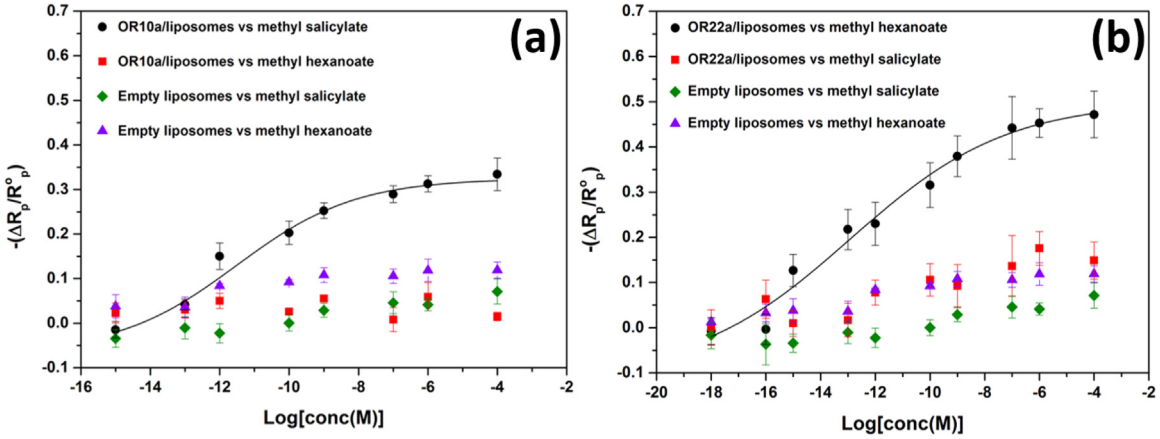

Fig. 5. Odorant detection using Or10a/liposome and Or22a/liposome immobilized EIS sensors (a) Dose response curve for the Or10a/liposome EIS sensor as a change in normalized polarization resistance with increasing concentration of the positive ligand, methyl salicylate, as well as response to the negative ligand methyl hexanoate. (b) Dose response curve for the Or22a/liposome EIS sensor as a change in normalized polarization resistance with increasing concentration of the positive ligand, methyl hexanoate, as well as response to the negative ligand methyl salicylate. Error bars; standard deviation (SD) were generated using four repeats. The response of an empty liposome immobilized EIS sensor to positive and negative ligands for both receptors is shown for comparison.

2.2.5. AFM, TEM and XPS measurements

Ti/Au coated ~40/50-nm microscope slides were cleaned using acid piranha solution (3:1 mixture of concentrated sulphuric acid (H_2SO_4) and hydrogen peroxide (H_2O_2)). The clean gold slides were air-dried and liposomes were immobilized on the surface using the procedure as described above. AFM images were taken after SAM, NHS/EDC coupling and liposome attachment using the AFM instrument, Cypher ES. Likewise, XPS study of bare, MHA-modified, NHS/EDC treated, liposomes immobilized and target odorant hybridized gold slides were carried out using the Kratos Axis DLD XPS system. For the TEM study, OrX/liposomes were sprayed on a Quantafoil TEM carbon grid followed by snap freezing in liquid ethane. A 120 kV Technai 12 TEM optimized for cryo-electron microscopy was used for imaging.

2.2.6. QCM-D measurements

Gold (100-nm thick) sensor crystals were sonicated in ethanol and milli-Q water for 15 min each. A 5:1:1 vol ratio of milli-Q water, ammonia (25%), and hydrogen peroxide (30%) was heated to 75 °C for 5 min and the sonicated crystals were placed in the heated solution for 5 min. Then the crystals were removed from the solution and rinsed thoroughly with milli-Q water before drying with nitrogen gas. The clean gold crystals were thiol functionalized by exposing them to a 2-mM ethanolic solution of MHA overnight followed by washing with ethanol solution in order to remove excess or loosely bound molecules. The SAM functionalized crystals were then placed into the Q-sense analyzer instrument (Biolin Scientific) chamber and the NHS/EDC, OrX/liposomes and odorants in PBS buffer solution were flowed over in that order. The changes in frequency (Δf) and dissipation (ΔD) values were measured before and after modification with OrX/liposomes.

2.2.7. EIS measurements

EIS measurements were done in a 3-electrode cell containing Ag/AgCl (3 M NaCl, 0.209 V vs. SHE) reference electrode, coiled platinum wire as a counter electrode and the gold disk as a working electrode at a fixed voltage of −0.7 using a PalmSens potentiostat. Degassed PBS was used as an electrolyte.

3. Results and discussion

Three *Drosophila melanogaster* OrX subunits (Or10a, Or22a and Or71a) (Dweck et al., 2015; Hallem and Carlson, 2006) were recombinantly overexpressed, purified and reconstituted into the lipid bilayers of artificial liposomes, and then immobilized onto sensor substrates. The experimental procedure for covalent attachment of OrXs/liposomes and binding of the target odorant molecules as monitored by EIS, is presented in Scheme 1.

3.1. Characterization of OrX/liposomes coupled to gold surfaces

TEM and AFM techniques were applied to investigate the size, shape and state of liposomes when they were bound to a surface. TEM images of the liposomes were taken on a carbon grid surface. Fig. 2(a) shows that the liposomes were well dispersed and still maintained their round vesicular shape. The average size of the liposomes was 128 ± 43 nm. AFM images in Fig. 1(b–f) show the change in surface morphology and roughness profile when the bare gold surface was modified with the OrX/liposomes. The bare gold surface consists of densely packed flat gold nano-crystals of various sizes with an average surface roughness value of around 2 nm. After deposition of the SAM and NHS/EDC activation, minor changes in the roughness were observed (see Supporting information page S5, Fig. S2). When liposomes were introduced, a change in surface morphology was observed, showing circular shaped liposomes of 119 ± 65 nm size on the surface and no rupture or lipid bilayer formation was observed (Jung et al., 2006). The increase in surface roughness relating to the height of liposomes (> 30 nm) (Fig. 1(d)) also demonstrates that liposomes were successfully attached to the gold surface. The difference in the liposomes height from AFM (30 nm) and TEM (> 100 nm) is likely due to flattening of the vesicles under the AFM imaging conditions. XPS analysis, showing the confirmation of covalent attachment of OrX/liposomes to gold surfaces, is presented in Supporting information (page S2-S4).

3.2. OrX-based biosensor for odorant detection using QCM-D

QCM-D has been previously used to monitor binding of ligands to mammalian odorant receptors and ion channels (Du et al., 2013; Ko and Park, 2005; Sung et al., 2006). The kinetics of surface functionalization with SAM, NHS-EDC, OrX/liposomes and their interactions with the target ligands were investigated by QCM-D. The SAM-modified gold crystals were placed into the QCM-D chamber, followed by flowing of slightly acidic NHS/EDC in PBS buffer (pH: 6.5) solution (Fig. 2). Due to the formation of N-hydroxysuccinimidyl ester between -COOH end groups of MHA and NHS/EDC coupling agents, a decrease in frequency (−16 Hz) was observed, corresponding to an increase in the mass of the surface (Orelma et al., 2012). This reaction was allowed to occur for some time until the signal became stable before PBS was used to remove unbound reagents, causing an increase in frequency to −3 Hz (7.5 ng/cm^2).

The flow of Or10a/liposomes solution into the system caused a large change in frequency corresponding to mass change caused by successful attachment of Or10a/liposomes. Also, the very high dissipation detected ($\Delta D = (48 \pm 1.0) \times 10^{-6}$) clearly shows that the liposomes are still intact without any rupture (Cho et al., 2010). Different concentrations of the odorant target, methyl salicylate in 1% DMSO in PBS buffer solution were then introduced into the QCM-D flow cell containing the Or10a/liposomes modified crystals. Note that the initial decrease in frequency, when buffer containing only 1% DMSO was introduced, is attributed to the bulk shift due to the addition of the co-solvent DMSO (Fig. 2(b)). Concentrations of methyl salicylate (8–1000 μM) resulted in an increase in frequency values corresponding to a decrease in mass, and a decrease in dissipation corresponding to increase in rigidity of the layer. We hypothesize these changes are related to the Or10a receptor acting like a channel even without the presence of Orco, causing release of water and ions from inside the vesicles. Furthermore, similar changes in frequency and dissipation were observed with two other receptors, Or22a and Or71a (see Khadka et al., 2018, Data in Brief article). The normalized dose response curves (Fig. 3) show target odorant detection from 8 μM which is *on par* with one study on *Caenorhabditis elegans* ODR-10 receptor (Du et al., 2013), but less sensitive than another ODR-10 study (pM) (Sung et al., 2006) and the rat I7 receptor in HEK293 cells (nM) (Ko and Park, 2005).

3.3. OrX-based biosensor for odorant detection using EIS

Detection of target odorants by the OrX/liposomes was further investigated by means of EIS which has been used to study ligand binding to mammalian odorant receptors and other membrane proteins (Benilova et al., 2008b; Hou et al., 2006, 2007; Khan et al., 2017; Silin et al., 2016).

Non-Faradaic EIS in the absence of any redox species was used to characterize our system. A polarization potential of −0.7 V was applied as that was found to be a potential where the gold electrode gave stable impedance signals. All of the EIS spectra were modeled by a Randles equivalent circuit, (see Khadka et al., 2018, Data in Brief article) where constant phase element (CPE) instead of ideal double layer capacitance (C_{dl}) was used to obtain the best fit. However, deviations from ideal capacitor were less than 10% and all CPE exponents (n) were greater than 0.9 in all cases. The fitted parameters, solution resistance (R_s), capacitance (Q) and polarization resistance (R_p), of Or10a, Or22a and Or71a sensors for all target ligand concentrations are tabulated and presented in Supporting information (page S6-S11, Table S3–S14). Fig. 4(a) presents the EIS response in terms of Nyquist plot for the Or71a/liposome functionalized sensors when exposed to a solution containing the target ligand 4-ethylguaiacol, at various concentrations. The Nyquist plot showed a decrease in EIS response after the addition of increasing concentration of 4-ethylguaiacol. A calibration curve (Fig. 4(b)) was obtained by plotting the change in polarization resistance $-(\Delta R_p/R^{\circ}_p)$ versus log [conc (Ligand)], as the sensor response. Here, R_p is the polarization resistance after Or71a/liposome-odorant interaction and R°_p is the polarization resistance before OR71a/liposome-odorant interaction. The sigmoidal fit for the Or71a dose response curve is shown in Fig. 4(b) and can be described by the sigmoidal equation, $y = 0.537/(1 + \exp(-0.520 \times (x + 14.83)))$, from which an Ec_{50} of 5.56 (± 0.62) x 10^{-15} M and a detection range of 10^{-17}–10^{-9} M can be calculated.

The calibration curve obtained by plotting the change in capacitance $-(\Delta Q/Q_o)$ versus log [conc (Ligand)] where Q_o and Q are the capacitance before and after Or71a/liposome-odorant interaction respectively, is shown in Khadka et al. (2018), Data in Brief article. A systematic decrease in the polarization resistance with the increase in the concentration of target ligand is caused by the change in dielectric or conductive properties of the electrode surface after the interaction of Or71a receptor with 4-ethylguaiacol molecules. Or71a/liposomes sensor responded to its ligand 4-ethyl guaiacol (Dweck et al., 2015) with the limit of detection (LOD) of 0.1 fM and did not respond significantly to the control ligand E2-hexenal. The sensor functionalized with the empty liposomes did not respond to either the positive and negative ligands.

We investigated the response of two other receptors, Or10a and Or22a, towards their respective target odorants (Hallem and Carlson, 2006). The sigmoidal fit for the Or10a dose responses curve is shown in Fig. 5(a) and can be described by the sigmoidal equation, $y = 0.312/(1 + \exp(-0.806 \times (x + 10.89)))$, from which Ec_{50} of 2.29 (± 0.96) × 10^{-12} M and a detection range of 10^{-13}–10^{-7} M can be calculated. Likewise, the Or22a dose response curve can be described by the sigmoidal equation, $y = 0.465/(1 + \exp(-0.532 \times (x + 12.08)))$, with an Ec_{50} of 1.12 (± 2.10) × 10^{-12} M and a detection range of 10^{-15}–10^{-7} M.

Fig. 5(a) showing the dose response curve for the Or10a/liposome based sensor towards methyl salicylate had a limit of detection (LOD) of 1 pM and no response towards the control ligand, methyl hexanoate. Fig. 5(b) shows that Or22a/liposomes based sensor responded sensitively to methyl hexanoate with a LOD of 1 fM, and no response towards methyl salicylate as a control ligand. The dose response curves in terms of capacitance change for both Or10a/liposome and Or22a/liposome EIS sensors are presented in Khadka et al. (2018). The EIS dose response plot of each OrX was generated from data acquired on four different electrodes and over an eight hour period (30 min incubation for each analyte concentration) at room temperature. This demonstrates that our OrX based EIS sensor is both reproducible and stable.

The Or71a/liposome and Or22a/liposome EIS sensors both exhibit fM LODs which are extremely sensitive when compared to insect OrX/Orco cell-based sensor approaches (LODs of 10 nM – 1 μM) (Misawa et al., 2010; Mitsuno et al., 2015; Termtanasombat et al., 2016) and mammalian odorant receptor EIS sensors (LODs of 10 pM) (Benilova et al., 2008b; Hou et al., 2007). This is a surprising finding as our sensor does not require the presence of the Orco subunit. It can be speculated that the OrX possibly acts as channel itself on its own, thus the binding with odorant molecules triggers the opening of an OrX channel, enabling the flow of ions and water out of the liposomes causing the impedance to decrease. In each of the presented graphs, empty liposomes do not respond to any of the target ligands demonstrating that the presence of each OrX is the key to the detection of their respective target ligand.

4. Conclusion

Insect odorant receptors (Or10a, Or22a and Or71a) from the common fruit fly, *Drosophila melanogaster*, were integrated into artificial liposomes and characterized by means of TEM and AFM analysis. The OrX/liposomes were not ruptured when they were immobilized onto gold surface and retained their vesicular form being round-shaped and uniformly dispersed. The successful modification of the gold surface with covalently attached OrX/liposomes was also confirmed by XPS and QCM-D studies.

From the odorant binding study using EIS, it was observed that these biosensor devices could sensitively and selectively detect odorants down to femtomolar levels. This work demonstrates, for the first time, that purified insect OrXs when reconstituted into artificial liposomes can still function when immobilized on a sensor surface. These results set a precedent for the use of insect odorant receptors in biosensors to exploit their ultrasensitivity and broad specificity range. The resulting sensors could form the core of smart real-time/point-of-use management tools for medical, food, agricultural and environmental applications. Moreover, the robustness of our OrX based biosensors also motivates to carry out future studies to detect mixed odorants and real samples, as well as understanding the mechanism of odorant binding in detail.

Acknowledgements

This work was supported by funding awarded to Dr Andrew Kralicek: the Kiwi Innovation Network (KiwiNET) inaugural Emerging Innovator Award, a Better Border Biosecurity (B3) grant (P/321022/06), and the New Zealand Institute for Plant and Food Research Limited (PFR) SSIF grant (P/321061/02); and to Dr Colm Carraher: a Rutherford fellowship from the New Zealand Royal Society. Roshan Khadka's PhD stipend was covered by the PFR SSIF grant, Jamal Cheema's PhD stipend was covered by the B3 grant.

Appendix A. Supporting information

Supplementary data associated with this article can be found in the online version at doi:10.1016/j.bios.2018.10.043.

References

Alfinito, E., Pousset, J., Reggiani, L., 2013. The electrical properties of olfactory receptors in the development of biological smell sensors. In: Crasto, C.J. (Ed.), Olfactory Receptors: Methods and Protocols. Humana Press, Totowa, NJ, pp. 67–83.

Angioy, A.M., Desogus, A., Barbarossa, I.T., Anderson, P., Hansson, B.S., 2003. Extreme sensitivity in an olfactory system. Chem. Senses 28 (4), 279–284.

Benilova, I., Chegel, V.I., Ushenin, Y.V., Vidic, J., Soldatkin, A.P., Martelet, C., Pajot, E., Jaffrezic-Renault, N., 2008a. Stimulation of human olfactory receptor 17-40 with odorants probed by surface plasmon resonance. Eur. Biophys. J. 37 (6), 807–814.

Benilova, I.V., Minic-Vidic, J., Pajot-Augy, E., Soldatkin, A.P., Martelet, C., Jaffrezic-Renault, N., 2008b. Electrochemical study of human olfactory receptor OR 17–40 stimulation by odorants in solution. Mater. Sci. Eng. C 28, 633–639.

Boyle, S.M., McInally, S., Ray, A., 2013. Expanding the olfactory code by *in silico* decoding of odor-receptor chemical space. Elife 2, e01120.

Carey, A.F., Wang, G.R., Su, C.Y., Zwiebel, L.J., Carlson, J.R., 2010. Odorant reception in the malaria mosquito *Anopheles gambiae*. Nature 464 (7285), 66–U77.

Carraher, C., 2013. Characterisation of the Insect Odorant Receptor Complex. Doctoral dissertation, ResearchSpace@ Auckland.

Carraher, C., Nazmi, A.R., Newcomb, R.D., Kralicek, A., 2013. Recombinant expression, detergent solubilisation and purification of insect odorant receptor subunits. Protein Expr. Purif. 90 (2), 160–169.

Cho, N.-J., Frank, C.W., Kasemo, B., Höök, F., 2010. Quartz crystal microbalance with dissipation monitoring of supported lipid bilayers on various substrates. Nat. Protoc. 5 (6), 1096.

Cook, B.L., Steuerwald, D., Kaiser, L., Graveland-Bikker, J., Vanberghem, M., Berke, A.P., Herlihy, K., Pick, H., Vogel, H., Zhang, S., 2009. Large-scale production and study of a synthetic G protein-coupled receptor: human olfactory receptor 17-4. Proc. Natl. Acad. Sci. USA 106 (29), 11925–11930.

Du, L., Wu, C., Peng, H., Zou, L., Zhao, L., Huang, L., Wang, P., 2013. Piezoelectric olfactory receptor biosensor prepared by aptamer-assisted immobilization. Sens. Actuators B: Chem. 187, 481–487.

Dweck, H.K., Ebrahim, S.A., Farhan, A., Hansson, B.S., Stensmyr, M.C., 2015. Olfactory proxy detection of dietary antioxidants in Drosophila. Curr. Biol. 25 (4), 455–466.

German, P.F., van der Poel, S., Carraher, C., Kralicek, A.V., Newcomb, R.D., 2013. Insights into subunit interactions within the insect olfactory receptor complex using FRET. Insect Biochem. Mol. Biol. 43 (2), 138–145.

Goldsmith, B.R., Mitala, J.J., Josue, J., Castro, A., Lerner, M.B., Bayburt, T.H., Khamis, S.M., Jones, R.A., Brand, J.G., Sligar, S.G., Luetje, C.W., Gelperin, A., Rhodes, P.A., Discher, B.M., Johnson, A.T., 2011. Biomimetic chemical sensors using nanoelectronic readout of olfactory receptor proteins. ACS Nano 5 (7), 5408–5416.

Guo, Z., Zine, N., Lagarde, F., Daligault, J., Persuy, M.A., Pajot-Augy, E., Zhang, A., Jaffrezic-Renault, N., 2015. A novel platform based on immobilized histidine tagged olfactory receptors, for the amperometric detection of an odorant molecule characteristic of boar taint. Food Chem. 184, 1–6.

Hallem, E.A., Carlson, J.R., 2006. Coding of odors by a receptor repertoire. Cell 125 (1), 143–160.

Hou, Y., Helali, S., Zhang, A., Jaffrezic-Renault, N., Martelet, C., Minic, J., Gorojankina, T., Persuy, M.-A., Pajot-Augy, E., Salesse, R., 2006. Immobilization of rhodopsin on a self-assembled multilayer and its specific detection by electrochemical impedance spectroscopy. Biosens. Bioelectron. 21 (7), 1393–1402.

Hou, Y., Jaffrezic-Renault, N., Martelet, C., Zhang, A., Minic-Vidic, J., Gorojankina, T., Persuy, M.A., Pajot-Augy, E., Salesse, R., Akimov, V., Reggiani, L., Pennetta, C., Alfinito, E., Ruiz, O., Gomila, G., Samitier, J., Errachid, A., 2007. A novel detection strategy for odorant molecules based on controlled bioengineering of rat olfactory receptor I7. Biosens. Bioelectron. 22 (7), 1550–1555.

Ihara, S., Yoshikawa, K., Touhara, K., 2013. Chemosensory signals and their receptors in the olfactory neural system. Neuroscience 254, 45–60.

Jung, H., Kim, J., Park, J., Lee, S., Lee, H., Kuboi, R., Kawai, T., 2006. Atomic force microscopy observation of highly arrayed phospholipid bilayer vesicle on a gold surface. J. Biosci. Bioeng. 102 (1), 28–33.

Kaiser, L., Graveland-Bikker, J., Steuerwald, D., Vanberghem, M., Herlihy, K., Zhang, S., 2008. Efficient cell-free production of olfactory receptors: detergent optimization, structure, and ligand binding analyses. Proc. Natl. Acad. Sci. USA 105 (41), 15726–15731.

Kaupp, U.B., 2010. Olfactory signalling in vertebrates and insects: differences and commonalities. Nat. Rev. Neurosci. 11 (3), 188–200.

Khadka, R., Aydemir, N., Carraher, C., Hamiaux, C., Cheema, Malmström, J., Kralicek, A., Travas-Sejdic, J., 2018. Preparation and characterization of insect odorant receptor based biosensors. Data Brief.

Khan, M.S., Dosoky, N.S., Mustafa, G., Patel, D., Berdiev, B., Williams, J.D., 2017. Electrophysiology of epithelial sodium channel (ENaC) embedded in supported lipid bilayer using a single nanopore chip. Langmuir 33 (47), 13680–13688.

Ko, H.J., Park, T.H., 2005. Piezoelectric olfactory biosensor: ligand specificity and dose-dependence of an olfactory receptor expressed in a heterologous cell system. Biosens. Bioelectron. 20 (7), 1327–1332.

Marshall, B., Warr, C.G., de Bruyne, M., 2010. Detection of volatile indicators of illicit substances by the olfactory receptors of *Drosophila melanogaster*. Chem. Senses 35 (7), 613–625.

Misawa, N., Mitsuno, H., Kanzaki, R., Takeuchi, S., 2010. Highly sensitive and selective odorant sensor using living cells expressing insect olfactory receptors. Proc. Natl. Acad. Sci. USA 107 (35), 15340–15344.

Mitsuno, H., Sakurai, T., Namiki, S., Mitsuhashi, H., Kanzaki, R., 2015. Novel cell-based odorant sensor elements based on insect odorant receptors. Biosens. Bioelectron. 65, 287–294.

Montagné, N., de Fouchier, A., Newcomb, R.D., Jacquin-Joly, E., 2015. Advances in the identification and characterization of olfactory receptors in insects. Prog. Mol. Biol. Transl. Sci. 55–80.

Nowotny, T., de Bruyne, M., Berna, A.Z., Warr, C.G., Trowell, S.C., 2014. *Drosophila* olfactory receptors as classifiers for volatiles from disparate real world applications. Bioinspir. Biomim. 9 (4).

Orelma, H., Johansson, L.-s., Filpponen, I., Rojas, O.J., Laine, J., 2012. Generic method for attaching biomolecules via avidin–biotin complexes immobilized on films of regenerated and nanofibrillar cellulose. Biomacromolecules 13 (9), 2802–2810.

Park, S.J., Kwon, O.S., Lee, S.H., Song, H.S., Park, T.H., Jang, J., 2012. Ultrasensitive flexible graphene based field-effect transistor (FET)-type bioelectronic nose. Nano Lett. 12 (10), 5082–5090.

Sato, K., Takeuchi, S., 2014. Chemical vapor detection using a reconstituted insect olfactory receptor complex. Angew. Chem. Int. Ed. Engl. 53 (44), 11798–11802.

Silin, V., Kasianowicz, J.J., Michelman-Ribeiro, A., Panchal, R.G., Bavari, S., Robertson, J.W., 2016. Biochip for the detection of bacillus anthracis lethal factor and therapeutic agents against anthrax toxins. Membranes 6 (3), 36.

Sung, J.H., Ko, H.J., Park, T.H., 2006. Piezoelectric biosensor using olfactory receptor protein expressed in Escherichia coli. Biosens. Bioelectron. 21 (10), 1981–1986.

Termtanasombat, M., Mitsuno, H., Misawa, N., Yamahira, S., Sakurai, T., Yamaguchi, S., Nagamune, T., Kanzaki, R., 2016. Cell-based odorant sensor array for odor discrimination based on insect odorant receptors. J. Chem. Ecol. 42 (7), 716–724.

Wang, G.R., Carey, A.F., Carlson, J.R., Zwiebel, L.J., 2010. Molecular basis of odor coding in the malaria vector mosquito *Anopheles gambiae*. Proc. Natl. Acad. Sci. USA 107 (9), 4418–4423.

Yang, H., Kim, D., Kim, J., Moon, D., Song, H.S., Lee, M., Hong, S., Park, T.H., 2017. Nanodisc-Based bioelectronic nose using olfactory receptor produced in Escherichia coli for the assessment of the death-associated odor Cadaverine. ACS Nano 11 (12), 11847–11855.